JOURNAL OF COMPUTATIONAL PHYSICS **132,** 299–311 (1997)
ARTICLE NO. CP965637

On Application of Fast and Adaptive Periodic Battle–Lemarie Wavelets to Modeling of Multiple Lossy Transmission Lines

Xiaojun Zhu,* Guangtsai Lei,† and Guangwen Pan

Department of Electrical Engineering, Arizona State University, Tempe, Arizona 85287-7206

Received August 7, 1995

In this paper, the continuous operator is discretized into matrix forms by Galerkin's procedure, using periodic Battle–Lemarie wavelets as basis/testing functions. The polynomial decomposition of wavelets is applied to the evaluation of matrix elements, which makes the computational effort of the matrix elements no more expensive than that of method of moments (MoM) with conventional piecewise basis/testing functions. A new algorithm is developed employing the fast wavelet transform (FWT). Owing to localization, cancellation, and orthogonal properties of wavelets, very sparse matrices have been obtained, which are then solved by the LSQR iterative method. This algorithm is also adaptive in that one can add at will finer wavelet bases in the regions where fields vary rapidly, without any damage to the system orthogonality of the wavelet basis functions. To demonstrate the effectiveness of the new algorithm, we applied it to the evaluation of frequency-dependent resistance and inductance matrices of multiple lossy transmission lines. Numerical results agree with previously published data and laboratory measurements. The valid frequency range of the boundary integral equation results has been extended two to three decades in comparison with the traditional MoM approach. The new algorithm has been integrated into the computer aided design tool, MagiCAD, which is used for the design and simulation of high-speed digital systems and multichip modules Pan *et al. IEEE Trans. Hyb. Manuf. Technol.* **15**(4), 465 (1992). © 1997 Academic Press

1. INTRODUCTION

The boundary integral equation method (BIE) has been widely used in the solution of electromagnetic problems. Since only the field quantities on the boundaries are required, the method is suitable for structures of conductors in layered and, more generally, piecewise homogeneous media. By employing the Green's function which takes into account the boundary conditions, the number of unknown variables in describing the system is kept to a minimum. The disadvantage of the integral equation method is that the coefficient matrices are dense. It takes $O(N^2)$ units of storage and $O(N^3)$ multiplications/divisions to solve the matrix equations. These factors restrict the application of the BIE to only electrically small problems.

*Current address: Candance Design Systems, San Jose, CA 95134.
†Current address: Mayo Foundation 2nd St. S.W., Rochester, MN 55905.

The wavelet expansion has proven to be an efficient method in the approximation of functions [2–5], thus providing an effective approach to the solution of integral equations. Because of the localized property, vanishing moment, and multiresolution analysis (MRA) of the wavelets, the resolution level of the solution, which is closely related to the grid size and the length of the wavelet series, can be chosen adaptively, according to the smoothness of the function at different locations. Beylkin *et al.* [6] first proposed a nonstandard form wavelet expansion of operators by projecting the operator onto a series of subspaces. Wavelets were employed as basis functions in the MoM (method of moments) [7–10].

Since in most practical problems the unknowns are defined on a finite domain, while most orthonormal wavelets are developed in $L^2(\Re)$, it is very inefficient to employ these wavelets as bases directly. To overcome this difficulty, the periodic wavelets [11, 12], intervallic wavelets [13], and weighted wavelets [14] are applied to practical electromagnetic problems.

Although sparse coefficient matrices have been obtained in the previous approaches, the computing effort in the evaluation of the matrix elements is much greater than that of the MoM with conventional piecewise basis functions. This is due to the poor regularity and lack of analytic expressions of most orthonormal wavelets, while the MRA requires accurate evaluations of the inner product integrals. The formulations of the previous approaches, although they keep many nice properties of wavelets, are not suitable for the fast evaluation of the matrix elements. In this paper, we formulate a fast and adaptive algorithm using a combined nonstandard and standard wavelet decomposition method, employing the Battle–Lemarie wavelets of different orders. In comparison with the widely used Daubechies' wavelets [15], the Battle–Lemarie wavelets have the advantage of symmetry and, more importantly, an approximate closed-form representation can be obtained by decomposing the wavelets into B-splines or polynomials of the same order. This is extremely useful especially when spectral integrals are involved. This method, as shown later, makes the wavelet expansion method no

0021-9991/97 $25.00

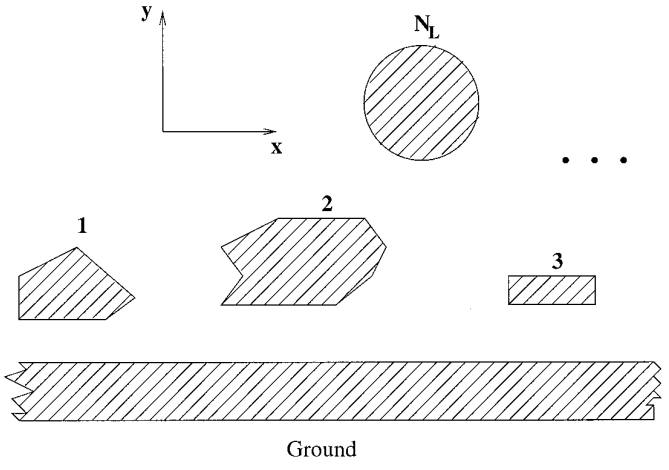

FIG. 1. N_L transmission lines of arbitrary cross section.

more time-consuming than Galerkin's procedure with B-spline or polynomial functions as basis functions.

In this paper, the LSQR iterative method is employed to solve these equations. Compared to other iteration methods, the LSQR method converges very quickly, and it does not require the sparse matrix to be a positive definite. A large amount of storage and computation time can be saved by storing the nonzero elements only. The wavelets for the finite energy functional space, $L^2([0, 1])$ [15, p. 305] are constructed from the Battle–Lemarie wavelets, from which the corresponding FWT is implemented.

As a direct application of the FWT, the frequency dependent inductance and resistance matrices of lossy transmission lines are evaluated. In the numerical section of this paper, it is demonstrated that the wavelet expansion method extends the valid frequency range of the MoM in two to three decades toward the lower end and one decade toward the higher end. The resulting matrices are sparse and well conditioned.

2. SOLUTION OF INTEGRAL EQUATIONS WITH FAST WAVELET EXPANSION METHOD

2.1. *Basic Formulation of Operator Equations*

Consider a 2D transmission line structure consisting of N_L conductors and one ground plane as shown in Fig. 1, where the ground plane can be a perfect conductor or of finite conductivity and finite dimensions. The fields inside and outside of the conductors can be decomposed into contributions from the TM (transverse magnetic) and TE (transverse electric) modes. Since the circumferential component of the electric current corresponding to the TE modes is usually much smaller than the longitudinal component, we only consider the contribution of the TM mode in this work. By assuming an equal potential at a given conductor cross section and by using Green's second identity, a set of surface integral equations can be derived. Denoting them in the form of operator equations, we have

$$\begin{aligned} &Z_E((\hat{n}\cdot\nabla)E_z)) + T_E(E_z + V_k) = 0 \\ &Z_I((\hat{n}\cdot\nabla)E_z)) + T_I(E_z) = 0, \quad k = 1, 2, ..., N_L, \end{aligned} \tag{1}$$

where subscripts E and I represent external and internal, respectively. E_z is the longitudinal component of the electric field on the conductor surfaces and V_k is the voltage on the kth transmission line. The operators are defined as

$$Z_{\mathrm{E}}(X) = \int_{L_e} dl' G_{\mathrm{E}}(\boldsymbol{\rho}, \boldsymbol{\rho}')X(\boldsymbol{\rho}'), \qquad \boldsymbol{\rho} \in L_e, \tag{2}$$

$$T_{\mathrm{E}}(X) = \int_{L_e} dl' (\hat{n}'\cdot\nabla_s') G_{\mathrm{E}}(\boldsymbol{\rho}, \boldsymbol{\rho}')X(\boldsymbol{\rho}'), \quad \boldsymbol{\rho} \in L_e, \tag{3}$$

$$Z_{\mathrm{I}}(X) = \int_{L_i} dl' G_{\mathrm{I}}(\boldsymbol{\rho}, \boldsymbol{\rho}')X(\boldsymbol{\rho}') \tag{4}$$

$$T_{\mathrm{I}}(X) = \int_{L_i} dl' (\hat{n}'\cdot\nabla_s') G_{\mathrm{I}}(\boldsymbol{\rho}, \boldsymbol{\rho}')X(\boldsymbol{\rho}'), \tag{5}$$

where L_i, $i = 1, 2, ..., N_L$ denotes the perimeter of the ith conductor; $L_e = \cup_{i=1}^{N_L} L_i$; $G_{\mathrm{I}}(\boldsymbol{\rho}, \boldsymbol{\rho}')$ is the 2D homogeneous Green's function given by

$$G_{\mathrm{I}}(\boldsymbol{\rho}, \boldsymbol{\rho}') = -\frac{j}{4\pi} H_0^{(2)}(k_i|\boldsymbol{\rho} - \boldsymbol{\rho}'|), \quad i = 1, 2, ..., N_L, \tag{6}$$

with $H_0^{(2)}(k_i|\boldsymbol{\rho} - \boldsymbol{\rho}'|)$ being the Hankel function (also referred to as the Bessel function of the third kind [16]) of the second kind, and

$$k_i = \omega\sqrt{\mu\varepsilon_i}$$

$$\varepsilon_i = \varepsilon_0\left(1 - j\frac{\sigma_i}{\omega\varepsilon_0}\right).$$

As it will be seen later, the computation of the matrix elements involves numerical evaluations of twofold integrals, which are very time consuming especially when the special functions of complex arguments are involved. Since most conductor contours can be approximated by a polygon, the inner product may be carried out analytically in the spectral domain [17]. In this case, only the inverse Fourier transform is needed. The spectral domain representation of the internal Green's function $G_I(\boldsymbol{\rho}, \boldsymbol{\rho}')$ is

$$\hat{G}_{\mathrm{I}}(\kappa, y, y') = \frac{e^{-\Gamma|y-y'|}}{2\Gamma}, \tag{7}$$

where

$$\Gamma = \sqrt{k_i^2 - \kappa^2}. \tag{8}$$

Under the quasi-static assumption, the external Green's function $G_E(\boldsymbol{\rho}, \boldsymbol{\rho}')$ reduces to

$$G_E(\boldsymbol{\rho}, \boldsymbol{\rho}') = -\frac{1}{2\pi} \ln |\boldsymbol{\rho} - \boldsymbol{\rho}'|. \tag{9}$$

To solve the above operator equations, a constraint is enforced,

$$\int_{L_i} (\hat{n} \cdot \nabla) E_i dl = -j\omega\mu I_i, \tag{10}$$

where I_i is the total electric current on the ith conductor and needs to be specified.

By solving these operator equations, the electric current distribution on the cross sections of the conductors can be obtained. Other field quantities can be evaluated from the electric field and its normal derivative on the boundaries. After the field quantities are solved, the resistance and inductance of the transmission lines can be computed straightforwardly. The ith diagonal element of the resistance/inductance matrices, namely, the self-resistance/inductance of the ith line, is calculated by setting the electric current I_i on the ith line, and $-I_i$, on the reference conductor (ground). Finally, after a long and tedious journey [19], we arrive at

$$R_{ii} = 2P_d/|I|^2 \tag{11}$$

$$L_{ii} = 4W_m/|I|^2, \tag{12}$$

where P_d is the dissipated electric power and W_m is the stored magnetic energy per unit length. After some mathematical manipulations, we end up with

$$P_d = \frac{1}{2\omega\mu} \oint_{L_e} \mathrm{Im}\{E_z \partial \tilde{E}_z\}\, dl \tag{13}$$

$$W_m = -\frac{1}{4\omega^2\mu} \oint_{L_e} \mathrm{Re}\{V_i \partial \tilde{E}_z\}\, dl, \tag{14}$$

where the tilde denotes the complex conjugate and $\partial E_z \triangleq \partial E_z/\partial n$. The mutual resistance and inductance are obtained from

$$\begin{aligned} R_{ij} &= \tfrac{1}{2}(R_{ii} + R_{jj} - 2P_d/I_i^2) \\ L_{ij} &= \tfrac{1}{2}(L_{ii} + L_{jj} - 4W_m/I_i^2), \end{aligned} \tag{15}$$

where P_d and W_m are the dissipated electric power and stored magnetic energy under conditions of $I_j = -I_i$.

2.2. *Galerkin's Solution of Operator Equations*

Consider an operator equation

$$(Tf)(x) = g(x), \tag{16}$$

where $f(x)$ is assumed to be a finite energy function. In the following discussion, we first consider the case where T is defined on $L^2(\Re)$.

With Galerkin's method, the operator equation is converted into a matrix form

$$[T^j][c^j] = [g^j], \tag{17}$$

where

$$T^j_{kk'} = \langle T(\phi_{jk'}), \phi_{jk} \rangle \tag{18}$$

$$g^j_k = \langle g, \phi_{jk} \rangle \tag{19}$$

with $\phi_{jk'}$ being the scaling functions. The approximate solution $f_j(x)$ may be expressed as

$$f_j(x) = \sum_k c^j_k \phi_{jk}. \tag{20}$$

The order of approximation depends on the resolution level j of the space in which T is discretized.

One method to calculate the matrix elements $T^j_{kk'}$ is the direct evaluation of the inner product, which is usually in the form of integrals. Generally, the scaling function $\phi(x)$ has a large support (i.e., the domain of nonzero $\phi(x)$) and oscillates rapidly, making this approach time-consuming.

The second approach is to use the B-spline decomposition of wavelets, as shown in Eq. (58) of the Appendix, yielding

$$T^j_{kk'} = \sum_i \sum_{i'} a_i a_{i'} Z^j_{i+k,i'+k'}, \tag{21}$$

where

$$Z^j_{i,k} = 2^j \langle T(\theta_N(2^j x - k)), \theta_N(2^j x - i) \rangle \tag{22}$$

and θ_N is the Nth-order B-spline defined in (48) of the Appendix. Since the B-spline function is very well behaved with small support and has a closed-form representation, the evaluation of $Z^j_{i,k}$ is much easier than the direct evaluation of $T^j_{kk'}$. This makes the wavelet expansion the same computatonal complexity as Galerkin's method with conventional piecewise bases.

The above procedures are for functions in $L^2(\Re)$. For

the problems defined on $L^2([0, 1])$, the periodic wavelets are needed. In this case, the matrix elements $\overline{T}^j_{kk'}$ are obtained from $T^j_{pp'}$ of the $L^2(\Re)$ as

$$\overline{T}^j_{kk'} = \sum_{\ell} \sum_{\ell'} T^j_{k+2^j\ell, k'+2^j\ell'}. \tag{23}$$

2.3. *Sparse Matrix Generation with a Fast Wavelet Transform (FWT)*

The continuous linear operator T can be approximated up to any order by its matrix form

$$T = \lim_{j\to\infty} T^j, \tag{24}$$

where T^j is a matrix of $N \times N$ ($N = 2^j$) and is defined as P_jTP_j with P_j being the projector on V_j. Since $V_{j+1} = V_j \oplus W_j$, we have

$$T^{j+1} = \begin{bmatrix} A^{jj} & B^{jj} \\ C^{jj} & T^j \end{bmatrix}, \tag{25}$$

where T^{j+1} is a matrix of $2N \times 2N$; A^{jj}, B^{jj}, and C^{jj} are block matrices of $N \times N$. The above procedure is also called the nonstandard decomposition of operators [6, 20]. In the numerical implementation, we applied the standard form of decomposition. As will be seen later in this section, the procedure here is very similar to the fast Fourier transform. We begin with a matrix of T^{j+1}, which is formed by $\langle T(\phi_{j+1,k'}), \phi_{j+1,k}\rangle$, i.e., the scaling functions for the basis and, also, testing. Since the scaling functions have nonzero moments, the resulting matrix T^{j+1} is relatively dense. But, after the FWT operations, the corresponding matrix will be very sparse.

Each entry of the matrix T^{j+1} is a square matrix, with their matrix elements being

$$\begin{aligned} A^{jj}_{kk'} &= \langle T(\psi_{jk'}), \psi_{jk}\rangle \\ C^{jj}_{kk'} &= \langle T(\psi_{jk'}), \phi_{jk}\rangle \\ B^{jj}_{kk'} &= \langle T(\phi_{jk'}), \psi_{jk}\rangle \\ T^j_{kk'} &= \langle T(\phi_{jk'}), \phi_{jk}\rangle, \end{aligned} \tag{26}$$

where the four submatrices represent the interaction between the sources and fields in different subspaces. Noticing that B^{jl} represents the interaction between W^j and V^l and that decomposing V^l into V^{l-1} and W^{l-1}, we obtain a recursive relation for B^{jl},

$$B^{j,l} = [A^{j,l-1}, B^{j,l-1}], \tag{27}$$

where $B^{j,l}$ is a matrix of $2^j \times 2^l$.

Similarly $C^{l,j}$ of $2^l \times 2^j$ is decomposed into

$$C^{l,j} = \begin{bmatrix} A^{l-1,j} \\ C^{l-1,j} \end{bmatrix}, \tag{28}$$

where

$$\begin{aligned} A^{l,j}_{k,k'} &= \langle T(\psi_{j,k'}), \psi_{l,k}\rangle \\ B^{j,l}_{k,k'} &= \langle T(\phi_{l,k'}), \psi_{j,k}\rangle \\ C^{l-1,j}_{k,k'} &= \langle T(\psi_{jk'}), \phi_{l-1,k}\rangle. \end{aligned} \tag{29}$$

By continuing the above process recursively, we can represent the operator in terms of wavelets. Since the wavelets are localized, most matrix elements for $[A]$, $[B]$, $[C]$ are nearly zero. As a result, a very sparse matrix may be formed.

The evaluation of matrix elements $A^{jj}_{kk'}$, $B^{ij}_{kk'}$, and $C^{jj}_{kk'}$ is much more time-consuming than the direct evaluation of $T^{j+1}_{kk'}$ at the highest resolution level by using the FWT.

From the MRA of the wavelets, the scaling functions and wavelets in V_j and W_j can be expressed by the scaling functions in V_{j+1} as

$$\begin{aligned} \phi_{jk} &= \textstyle\sum_n h_{n-2k}\phi_{j+1,n} \\ \psi_{jk} &= \textstyle\sum_n g_{n-2k}\phi_{j+1,n}, \end{aligned} \tag{30}$$

where h_k, g_k are the corresponding low-pass and band-pass filter coefficients specified by the specific wavelets used. Substituting (30) back to (26), we have

$$\begin{aligned} A^{jj}_{kk'} &= \langle T(\psi_{jk'}), \psi_{jk}\rangle \\ &= \left\langle T\left(\sum_m g_{m-2k'}\phi_{j+1,m}\right), \sum_n g_{n-2k}\phi_{j+1,n}\right\rangle \\ &= \sum_m \sum_n g_{m-2k'}g_{n-2k}\langle T(\phi_{j+1,m}), \phi_{j+1,n}\rangle. \end{aligned} \tag{30}$$

From the definition of $T^{j+1}_{kk'}$, we arrive at

$$A^{jj}_{kk'} = \sum_m \sum_n g_{m-2k'}g_{n-2k}T^{j+1}_{mn}. \tag{32}$$

Similarly, for $B^{jl}_{kk'}$, we have the following relation

$$\begin{aligned} B^{j,l-1}_{kk'} &= \langle T(\phi_{l-1,k'}), \psi_{jk}\rangle \\ &= \sum_m h_{m-2k'}\langle T(\phi_{l,m}), \psi_{jk}\rangle \\ &= \sum_m h_{m-2k'}B^{j,l}_{k,m}. \end{aligned} \tag{33}$$

It can be clearly seen that all the matrix elements may be

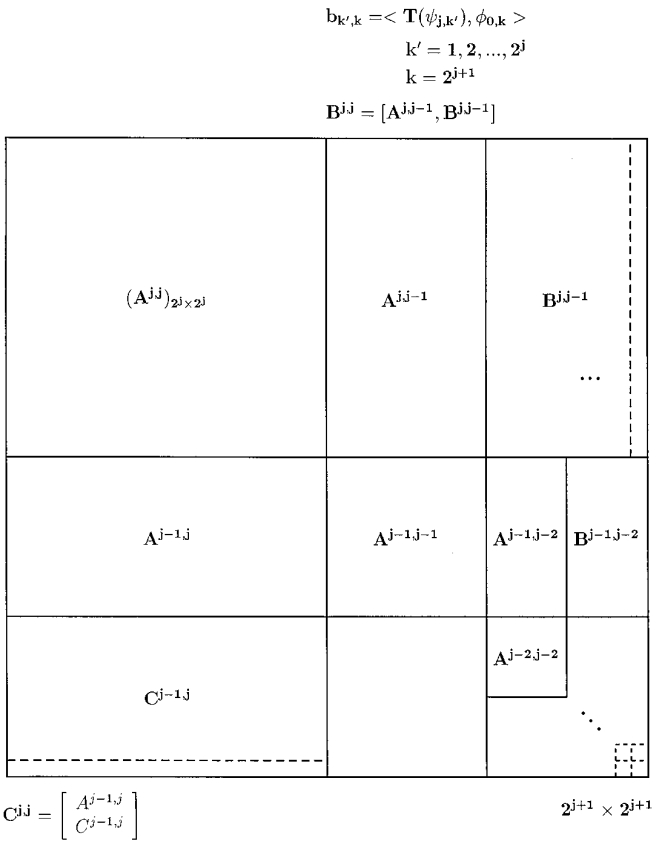

FIG. 2. Schematic diagram of the FWT structure.

generated from T^{j+1}. Since the above algorithm is similar to the fast Fourier transform (FFT), it is referred to as the FWT.

By using FWT, all other submatrices can be computed as

$$\begin{aligned} B^{jj}_{kk'} &= \sum_m \sum_n g_{m-2k} h_{n-2k'} T^{j+1}_{mn} \\ C^{jj}_{kk'} &= \sum_m \sum_n h_{m-2k} g_{n-2k'} T^{j+1}_{mn} \\ T^{j}_{kk'} &= \sum_m \sum_n h_{m-2k} h_{n-2k'} T^{j+1}_{mn'} \\ A^{j,l-1}_{k,k'} &= \sum_m g_{m-2k'} B^{jl}_{km} \\ C^{l-1,j}_{k,k'} &= \sum_m h_{m-2k} C^{lj}_{mk'} \\ A^{l-1,j}_{k,k'} &= \sum_m g_{m-2k} C^{lj}_{mk'}. \end{aligned} \tag{34}$$

For ease of reference, the FWT algorithm described in this section is illustrated graphically in Fig. 2.

2.4. *Wavelet Expansion of Periodic Operators*

For a periodic operator $\overline{T}$ defined on $L^2([0, 1])$, the periodic wavelets are required in the wavelet expansion [15]. Consequently, all formulas in the previous subsection need to be modified accordingly.

Similar to T, the periodic operator $\overline{T}$ can also be expanded in the sequential form as

$$\overline{T}^{j+1} = \begin{bmatrix} \overline{A}^{jj} & \overline{B}^{jj} \\ \overline{C}^{jj} & \overline{T}^{j} \end{bmatrix}, \tag{35}$$

where each of the four submatrices is a $2^j \times 2^j$ square matrix, and

$$\begin{aligned} \overline{A}^{jj}_{kk'} &= \langle \overline{T}(\overline{\psi}_{jk'}), \overline{\psi}_{jk} \rangle \\ \overline{C}^{jj}_{kk'} &= \overline{T}(\overline{\psi}_{jk'}), \overline{\phi}_{jk} \rangle \\ \overline{B}^{jj}_{kk'} &= \langle \overline{T}(\overline{\phi}_{jk'}), \overline{\psi}_{jk} \rangle \\ \overline{T}^{j}_{kk'} &= \langle \overline{T}(\overline{\phi}_{jk'}), \overline{\phi}_{jk} \rangle \\ \overline{B}^{jl} &= [\overline{A}^{j,l-1}, \overline{B}^{j,l-1}] \\ \overline{C}^{l,j} &= \begin{bmatrix} \overline{A}^{l-1,j} \\ \overline{C}^{l-1,j} \end{bmatrix} \end{aligned} \tag{36}$$

with

$$\overline{A}^{l,j}_{k,k'} = \langle \overline{T}(\overline{\psi}_{j,k'}), \overline{\psi}_{l,k} \rangle. \tag{38}$$

Note that the inner product is defined on interval [0, 1] as

$$\langle f, g \rangle = \int_0^1 f(x) g(x)\, dx. \tag{39}$$

The FWT is still applicable to the evaluation of the matrix elements. More efficiently, instead of evaluating $\overline{A}^{jj}_{kk'}, \overline{B}^{jj}_{kk'}, \overline{C}^{jj}_{kk'}$, and $\overline{T}^{j}_{kk'}$ from $\overline{T}^{j+1}_{kk'}$, we utilize $B^{jj}_{kk'}, C^{jj}_{kk'}$, and $T^{j}_{kk'}$ of the previous section. Following the periodization procedure, we have

$$\begin{aligned} \overline{A}^{l,j}_{kk'} &= \sum_\ell \sum_{\ell'} A^{l,j}_{(k+2^l\ell),(k'+2^j\ell')} \\ \overline{B}^{jl}_{kk'} &= \sum_\ell \sum_{\ell'} B^{jl}_{(k+2^j\ell),(k'+2^l\ell')} \\ \overline{C}^{lj}_{kk'} &= \sum_\ell \sum_{\ell} C^{lj}_{(k+2^l\ell),(k'+2^j\ell')} \\ \overline{T}^{j}_{kk'} &= \sum_\ell \sum_{\ell'} T^{j}_{(k+2^j\ell),(k'+2^j\ell')}. \end{aligned} \tag{40}$$

In the above equations, the length of summation with respect to ℓ and ℓ' depends on the resolution level j and the subscripts k, k'. It can be verified that the length of summation with respect to ℓ, ℓ' is at most 2, if $2^{-j} \max(L_\phi, L_\psi) \le 1$, where L_ϕ, L_ψ are the support or truncation length of the scaling function and mother wavelet.

2.5. *Expansion of Operators with Periodic Wavelets*

Thus far, we may see that all of the operators are defined on the conductor surfaces (contours) with arbitrary shape. Employ the following mapping relation

$$L_i \xleftarrow{\boldsymbol{\rho}=\boldsymbol{f}_i(x)} [0,1]_i, \tag{41}$$

where $([0,1])_i$ denotes the segment $[0,1]$ on the ith axis of an N_L-dimensional coordinate system. Hence, each conductor surface (contour) is mapped to a segment on an axis of the N_L-dimensional system, and the field quantities are periodic with period 1.

With such a mapping scheme, the operators are converted into a set of new period operators of the following forms

$$\begin{aligned}
\overline{Z}_E(X) &= \sum_{j=1}^{N_L} \int_0^1 G_E(\boldsymbol{f}_i(x),\boldsymbol{f}_j(x'))\alpha_j(x')X(x')\,dx' \\
&\qquad \text{if } x \in [0,1]_i \\
\overline{T}_E(X) &= \sum_{j=1}^{N_L} \int_0^1 (\hat{n}'\cdot\nabla_s')G_E(\boldsymbol{f}_i(x),\boldsymbol{f}_j(x'))\alpha_j(x')X(x')\,dx' \\
&\qquad \text{if } x \in [0,1]_i \\
\overline{Z}_I(X) &= \int_0^1 G_I(\boldsymbol{f}_i(x),\boldsymbol{f}_i(x'))\alpha_j(x)X(x')\,dx', \\
&\qquad x \in [0,1]_i \\
\overline{T}_I(X) &= \int_0^1 (\hat{n}'\cdot\nabla_s')G_I(\boldsymbol{f}_i(x),\boldsymbol{f}_i(x'))\alpha_j(x)X(x')\,dx', \\
&\qquad x \in [0,1]_i
\end{aligned} \tag{42}$$

where $\alpha_j(x)$, $j = 1, 2, ..., N_L$, is defined as

$$\alpha_j(x) = \left|\frac{\partial \boldsymbol{f}_j(x)}{\partial x}\right|. \tag{43}$$

Although the periodic operators are defined in the N_L-dimensional space, their domain and range are defined only on the segments $\bigcup_{i=1}^{N_L}[0,1]_i^p$, which is the union of N_L disjoint one-dimensional spaces. This makes the problem no more difficult than the one-dimensional case.

Using the periodic wavelet bases as defined in Eqs. (64) and (65) of the Appendix, the electric field and its normal derivative on the conductor boundaries are expressed as

$$E_{z,i}^n = \sum_{k=0}^{2^{j_0}-1} c_{j_0,k}^i \phi_{j_0,k} + \sum_{j=j_0}^{n-1}\sum_{k=0}^{2^j-1} d_{j,k}^i \psi_{j,k} \tag{44}$$

$$\partial E_{z,i}^n = \sum_{k=0}^{2^{j_0}-1} \partial c_{j_0,k}^i \phi_{j_0,k} + \sum_{j=j_0}^{n-1}\sum_{k=0}^{2^j-1} \partial d_{j,k}^i \psi_{j,k}, \tag{45}$$

where $i = 1, 2, ..., N_L$; $E_{z,i}^n$, $\partial E_{z,i}^n$ denote the approximation of the electric field and its normal derivative for the ith conductor at resolution level n; $c_{j_0,k}^i$, $\partial c_{j_0,k}^i$ are the coefficients for the scaling functions at resolution level j_0; $\partial d_{j,k}^i$ are the coefficients for the wavelets at level j.

Employing the wavelet expansion method for periodic operators and assembling the matrices together, the unknown coefficients $c_{j_0,k}^i$, $\partial c_{j_0,k}^i$, $d_{j,k}^i$, and $\partial d_{j,k}^i$ can be solved.

From the orthonormal property of the wavelets, we have

$$\oint_{L_i} dl\,\{E_z\overline{\partial E_z}\} = \sum_{k=0}^{2^{j_0}-1} c_{j_0,k}^i \overline{\partial c_{j_0,k}^i} + \sum_{j=j_0}^{n_m^i-1}\sum_{k=0}^{2^j-1} d_{j,k}^i \overline{\partial d_{j,k}^i}, \tag{46}$$

where $n_m^i = \min\{n_E^i, n_{\partial E}^i\}$, n_E^i and $n_{\partial E}^i$ are the highest resolution level for the wavelet expansion of the electric field and its normal derivative on the ith conductor, and

$$\oint_{L_i} dl\,\partial E = \sum_{k=0}^{2^{j_0}-1} \partial c_{j_0 k}^i. \tag{47}$$

It can be seen that all the integrals have been converted into summations.

2.6. *Solution of Matrix Equations by LSQR Method*

Following the above procedures we end up with a set of linear equations as $\mathbf{Ax} = \mathbf{b}$. The direct solution of the matrix equation by Gaussian elimination requires $O(n^3)$ multiplications/divisions and $O(n^2)$ units of storage. This method is not suitable for the sparse matrices because the sparsity of the matrices is destroyed during the computation. Although there are many sparse matrix equation solvers, most of them require the coefficient matrix to be positive definite, which is not satisfied in many practical problems. Here the LSQR iterative method [21] is employed to solve the matrix equations.

Analytically, the LSQR method is equivalent to the conjugate gradient method (CG), except for some more favorable properties. In principle, the CG method converges for at most n iterations, although it may be far more or far less than the number of iterations, n, depending on the property of the matrix. The LSQR method is based on the idea of dividing the solution process into the direct part and the iterative part. The direct part provides a better preconditioned matrix for the iterative part so that fast convergence can be achieved. In the LSQR method, the bi-diagonalization procedures are used for the direct part. For more details of the algorithm, readers are referred to [21, 22].

The main computation involved in the LSQR algorithm is the multiplication of a matrix with a vector. The sparsity of the matrices can be fully exploited. Since most of the matrix elements are zero, a large amount of storage can

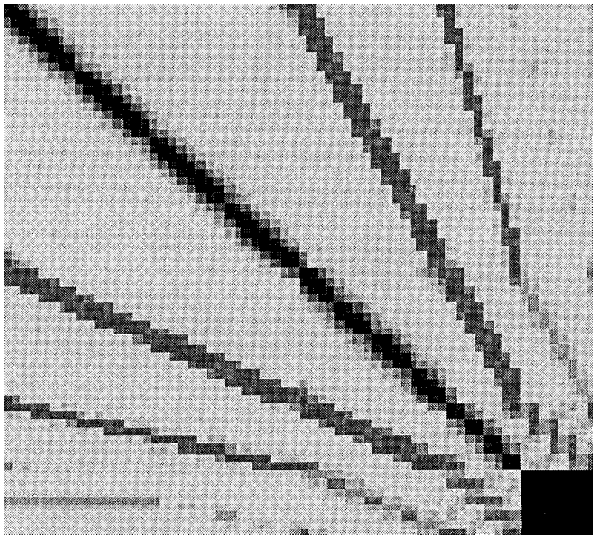

FIG. 3. First quarter of coefficient matrix $[Z_e]$ by four level wavelet expansion with Franklin wavelets.

be saved by storing the nonzero elements only. Static storage and dynamic storage are the two main categories of storage schemes. Since the sparse matrices are not changed in the least-square QR decomposition, the static storage scheme is adopted due to its ease of access and economy of memory [23, 24].

3. NUMERICAL RESULTS AND DISCUSSION

In this section, the FWT is employed to calculate the resistance and inductance matrices of lossy transmission lines of arbitrary cross-section shapes.

EXAMPLE 1. *Dual lines.* The first example is a pair of parallel square transmission lines in free space. The dimensions of the conductors are 2 mm $\times$ 2 mm, with 2 mm spacing. The conductors are made of copper with $\sigma = 5.6 \times 10^7$ S/m. Franklin wavelets are used and truncated at $L_\phi = 16$, and the lowest resolution level is chosen to be $j_0 = 3$.

To demonstrate the advantage of the wavelet expansion method, we plotted in Fig. 3 a quarter of the coefficient matrix $[Z_e]$ in terms of the magnitude obtained from the FWT method. The magnitude in the figures has been quantized and is represented by an 8-bit gray level image. The coefficient matrix is obtained from four-level wavelet expansion with Franklin wavelets. It can be seen that the wavelet expansion method results in a very sparse coefficient matrix. In contrast, the coefficient matrix from the Galerkin method would result in a completely dark figure. The sparsity reduces the memory requirement, thus allowing us to solve electrically large problems. The iterative method of the sparse matrix solver LSQR is effectively used.

TABLE I

Comparison of Matrix Size between MoM and Wavelet Expansion

Grid size	$L_{\text{MoM}}(nH)$	N_{MoM}	$L_{\text{W.E.}}(nH)$	$N_{\text{W.E.}}$
2^{-3}	430.2	34	429.5	34
2^{-4}	573.0	66	572.8	66
2^{-5}	595.6	130	594.5	98
2^{-6}	599.1	258	598.8	130

To illustrate the advantage of the wavelet expansion method over the conventional MoM, the performance of the two methods are compared in Table I for the problem in Example 1 with the frequency chosen to be 1 Hz. Using the normalized frequency [25], 1 Hz here corresponds to 4.2 MHz of typical geometry in the on chip structures. In the table, MoM denotes the method of moments with triangle functions as both basis and testing functions, while W.E. denotes the wavelet expansion method employing Franklin wavelets with only two wavelets added to each conductor corner at each of the two additional levels; N_{MoM} and $N_{W.E.}$ denote the matrix size obtained by the two methods respectively; L_{MoM} and $L_{W.E.}$ are the resulting inductance values in nano Henrys from the two methods. From the table one can see that as the grid refines, the matrix size by the MoM increases exponentially, while the matrix size for the wavelet expansion increases only linearly. To achieve the same accuracy, the matrix size for the wavelet expansion is much smaller than that of the MoM with triangular basis functions when the grid size is small.

EXAMPLE 2. *Triple line system.* The second example deals with a lossy transmission line system, which consists of three identical rectangular conductors of equal height above an infinite ground plane. The dimensions of the conductors are $w \times t = 100\ \mu\text{m} \times 30\ \mu\text{m}$, with 100 μm edge-to-edge spacing and 30 μm height from the ground plane, i.e., Fig. 5 in [19]. The ground plane is approximated by a conductor with a cross section of $w \times t = 1000\ \mu\text{m} \times 300\ \mu\text{m}$. The self and mutual resistances of the three transmission lines versus frequency are plotted in Fig. 4, while the self and mutual inductances are plotted in Fig. 5. The MoM results are also plotted in Fig. 4 and Fig. 5. Since the standard MoM is very sensitive to numerical errors, the mutual resistances, R12 and R13, and mutual inductance L13 are not stable. Therefore, no MoM curves of the mutual R or L13 can be plotted. It can be clearly seen that by employing the W.E., the frequency range has been extended two to three decades towards the low frequency end.

EXAMPLE 3. *Hughes aluminum/polyimide MCM test coupon.* To verify the new algorithm further, a set of labora-

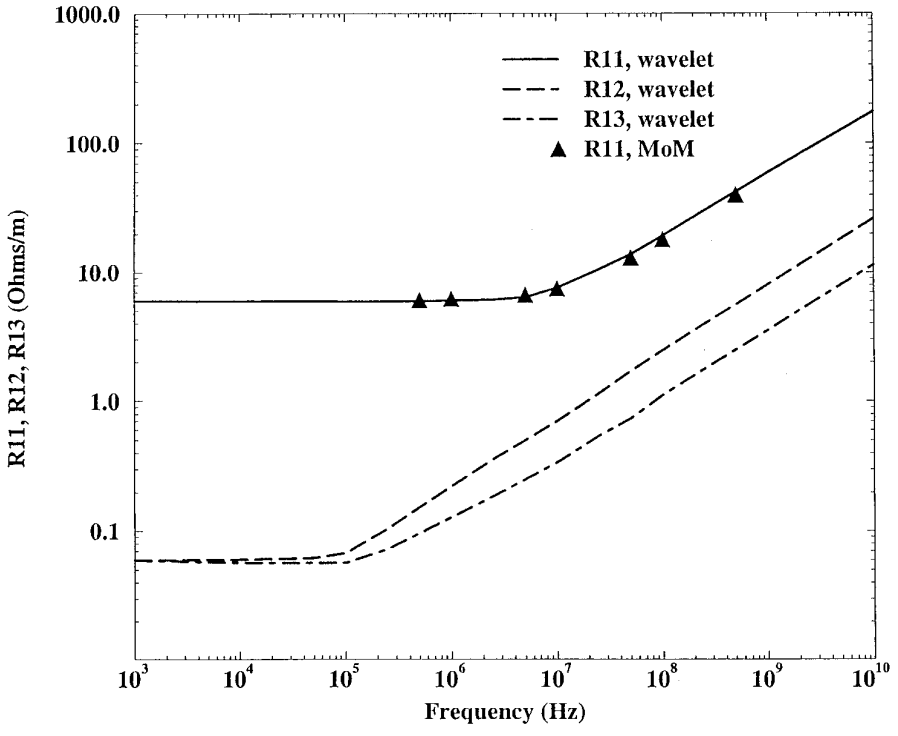

FIG. 4. Frequency dependent self and mutual resistances of three rectangular wires over a ground plane.

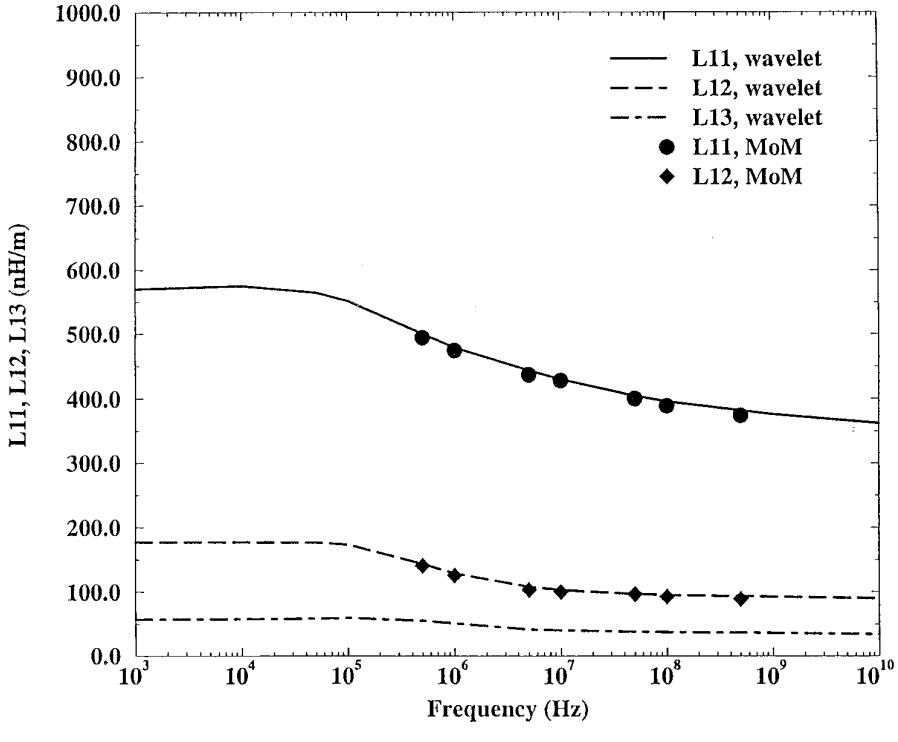

FIG. 5. Frequency dependent self and mutual inductancies of three rectangular wires over a ground plane.

TABLE II

Comparison of Measurements against Computations

Line parameter (1 in length)	Group 1	Group 2
H	10 μm	20 μm
Inductance L (nH/m)		
Hughes measured	8.4	10.5
Quasi-static	6.0	8.7
Wavelets	8.0	10.57
Resistance R (Ohms/m)		
Hughes measured	9.34	8.14
Quasi-static	14.07	12.37
Wavelets	8.85	8.53
Impedance Z_c (Ohms)		
Hughes measured		
LC meter	48.1	64.8
TDR	50.3	64.7
Quasi-static (real part)	39.0	59.0
Wavelets (real part)	45.0	65.03

tory measurements is compared with our numerical solutions in Table II. The test coupon consists of two groups of single buried strip lines. The dimensions are $w \times t = 25\ \mu\text{m} \times 5\ \mu\text{m}$ for the strips, and $w \times t = 125\ \mu\text{m} \times 5\ \mu\text{m}$ for the bottom ground plane. All conductors are made of aluminum with conductivity $\sigma = 3.0 \times 10^7$ S/m. The height of the strip line to the ground plane H is 10 μm for group 1 and 20 μm for group 2. The operating frequency is $f =$ 200 MHz. The traditional quasi-static model [26] neglects the internal inductance and assumes that current is only flowing on the surface region of the cross section. This model may well underestimate the inductance value near 30% and overestimate the resistance value up to 50%.

4. CONCLUSION

In this paper, the periodic Battle–Lemarie wavelets are constructed and applied to the solution of boundary integral equations in electromagnetics. A fast wavelet transform algorithm is developed. By using the polynomial decomposition of wavelets, the computational complexity in the evaluation of the coefficient matrix elements is equivalent to that of Galerkin's method with the same order polynomial bases. Since the resulting coefficient matrices are very sparse, memory storage and computational effort are significantly reduced when employing dynamic programming and the LSQR iterative method. The new algorithm is applied to the computation of frequency-dependent resistance and inductance matrices of lossy transmission lines. Good agreement with previously published data and laboratory measurements is observed. The new method can be applied to electrically large problems where the conventional method of moments is not applicable.

APPENDIX: CONSTRUCTION OF ORTHONORMAL WAVELET BASES

A.1. *Construction of Battle–Lemarie Wavelets*

The Nth-order Lemarie–Meyer wavelet is constructed from a linear combination of the translations of the Nth-order B-spline function $\theta_N(x)$. The Fourier transform of $\theta_N(x)$ is

$$\hat{\theta}_N(\omega) = e^{-j(N\omega/2)} \left(\frac{\sin(\omega/2)}{\omega/2} \right)^{N+1}. \tag{48}$$

After orthonormalization [27–29], the scaling function, which is also referred to as the father wavelet, $\phi(x)$ can be obtained by finding the inverse Fourier transform of

$$\hat{\phi}(\omega) = e^{-j\kappa(\omega/2)} \left(\frac{\sin(\omega/2)}{\omega/2} \right)^{N+1} a_N^{-1/2}(\omega), \tag{49}$$

where $\kappa = 0$ if N is odd, or $\kappa = 1$ if N is even, with

$$a_N(\omega) = \sum_k |\hat{\theta}_N(\omega + 2\pi k)|^2. \tag{50}$$

The functions $a_N(\omega)$ for the first- to fifth-order Battle–Lemarie wavelets are given in Table III.

The mother wavelet is obtained from the Fourier transform

$$\hat{\psi}(\omega) = e^{-j\omega/2} \overline{m_0\left(\frac{\omega}{2} + \pi\right)}\, \hat{\phi}\left(\frac{\omega}{2}\right), \tag{51}$$

where the overline denotes the complex conjugate and

TABLE III

Function $a_N(\omega)$ for the First- to Fifth-Order Battle–Lemarie Wavelets

N	$a_N(\omega)$
1	$1 - \frac{2}{3}\sin^2(\omega)$
2	$(2\cos^4(\omega) + 11\cos^2(\omega) + 2)/15$
3	$(64\cos^6(\omega) + 1824\cos^4(\omega) + 2880\cos^2(\omega) + 272)/5440$
4	$(256\cos^8(\omega) + 31616\cos^6(\omega) + 185856\cos^4(\omega) + 137216\cos^2(\omega) + 7936)/362880$
5	$(1024\cos^{10}(\omega) + 518656\cos^8(\omega) + 8728580\cos^6(\omega) + 21253400\cos^4(\omega) + 9061380\cos^2(\omega) + 353793)/399168$

$$m_0\left(\frac{\omega}{2}\right) = \frac{\hat{\phi}(\omega)}{\hat{\phi}(\omega/2)}. \tag{52}$$

Since all orthonormal wavelets, except the Haar system, do not have an explicit closed form representation, they are usually represented by the two level relations

$$\phi(x) = \sum_{n=-\infty}^{\infty} h_n \phi_{1,n} \tag{53}$$

$$\psi(x) = \sum_{n=-\infty}^{\infty} g_n \phi_{1,n}, \tag{54}$$

where h_n, g_n are constant coefficients for the specified wavelet system and

$$\phi_{j,k} = 2^{j/2}\phi(2^j x - k) \tag{55}$$

$$\psi_{j,k} = 2^{j/2}\psi(2^j x - k). \tag{56}$$

Coefficients h_n, g_n are the corresponding low-pass and band-pass filter coefficients and can be evaluated from the MRA of the wavelets as

$$\begin{aligned} h_n &= \langle \phi_{0,0}, \phi_{1,n} \rangle \\ g_n &= (-1)^{1-n} h_{1-n}. \end{aligned} \tag{57}$$

For the Franklin wavelets, or the first-order Lemarie–Meyer wavelets, the filter coefficients h_n are given in Table III.

The scaling function $\phi(x)$ and mother wavelet $\psi(x)$ of the first- to third-order Battle–Lemarie wavelets are shown in Figs. 6 and 7.

A.2. *Decomposition of Battle–Lemarie Wavelets*

Two disadvantages of wavelets are the lack of closed-form representation and fast oscillation, which make numerical computations very expensive if the wavelets are employed as basis functions directly. By observing the construction process of the Battle–Lemarie wavelets we see that both the scaling functions and the wavelets are the composition of the dilations and translations of the B-spline functions. This fact allows us to express the wavelets by a set of B-spline functions, namely

$$\phi(x) = \sum_k a_k \theta_N(x - k), \tag{58}$$

where the coefficients a_k are obtained by expanding $a_N^{-1/2}(\omega)$ into the Fourier series.

Similarly, the wavelets are represented as

$$\psi(x) = \sum_k b_k \theta_N(2x - k - 1), \tag{59}$$

where b_k is obtained by using (54),

$$b_k = \sqrt{2} \sum_n g_n a_{k-n}. \tag{60}$$

Since the scaling function and mother wavelet are symmetric and anti-symmetric, we have

$$\begin{aligned} a_{-k} &= a_k \\ b_{-k} &= (-1)^{N-1} b_k. \end{aligned} \tag{61}$$

For the Franklin wavelets, the scaling function and mother wavelet are decomposed into a sequence of triangles,

$$\begin{aligned} \phi(x) &= \Sigma_k a_k T(x - k) \\ \psi(x) &= \Sigma_k b_k T(2x - k - 1), \end{aligned} \tag{62}$$

where

$$T(x) = \begin{cases} 1 - |x| & \text{if } |x| < 1, \\ 0 & \text{otherwise.} \end{cases} \tag{63}$$

The coefficients a_k and b_k are given in Tables IV and V.

A.3. *Construction of Wavelets on $L^2([0, 1])$*

So far, the wavelets are constructed as sets of orthonormal bases for $L^2(\Re)$. For many practical problems, the unknowns are defined on a finite interval. Thus, if these wavelets are applied directly, the end points of the interval must be treated carefully. Otherwise, the orthogonality of the system and the sparsity of the matrices will be degraded [10]. In this section the periodic orthonormal wavelet bases for the periodic space $L^2([0, 1])$ are constructed.

The periodic wavelets are the simplest orthonormal wavelets on a segment. The scaling function and mother wavelet for $L^2([0, 1])$ can be constructed from the available orthonormal wavelets for $L^2(\Re)$, using the fact that $L^2([0, 1])$ is a subspace of $L^2(\Re)$. Denoting the periodic scaling functions and wavelets on the segment [0, 1] as $\overline{\phi}_{jk}$ and $\overline{\psi}_{jk}$, we have

$$\overline{\phi}_{jk} = \sum_{\ell \in Z} \phi_{jk}(x + \ell) \tag{64}$$

$$\overline{\psi}_{jk} = \sum_{\ell \in Z} \psi_{jk}(x + \ell), \tag{65}$$

where $j \geq 0$, $k = 0, 1, ..., 2^j - 1$.

By assuming that the lowest resolution level is high

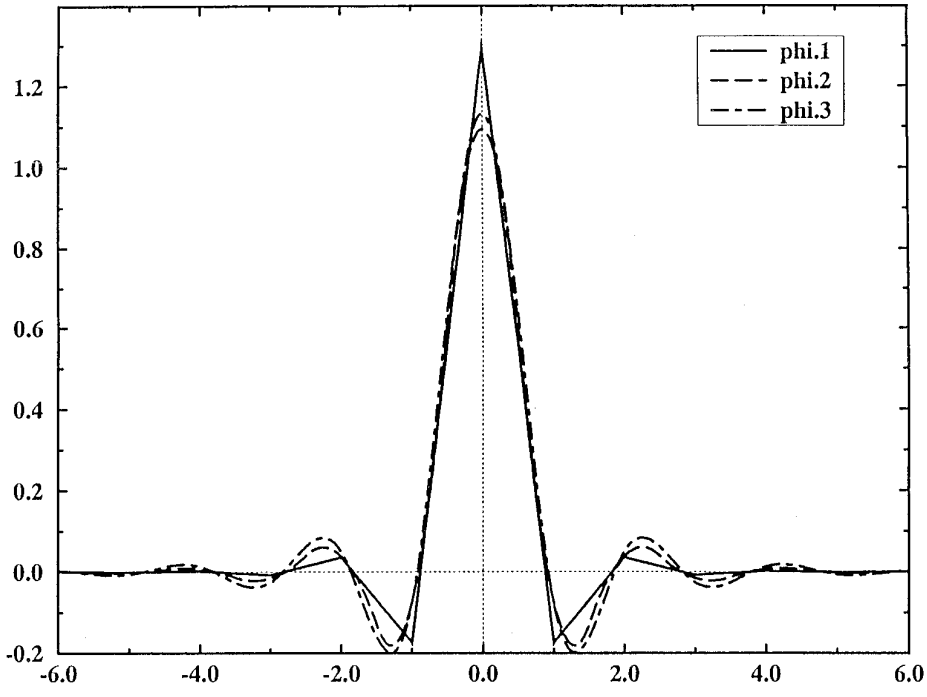

FIG. 6. Scaling function of the Franklin, quadratic, and cubic Lemarie–Meyer wavelets for $L^2(\Re)$.

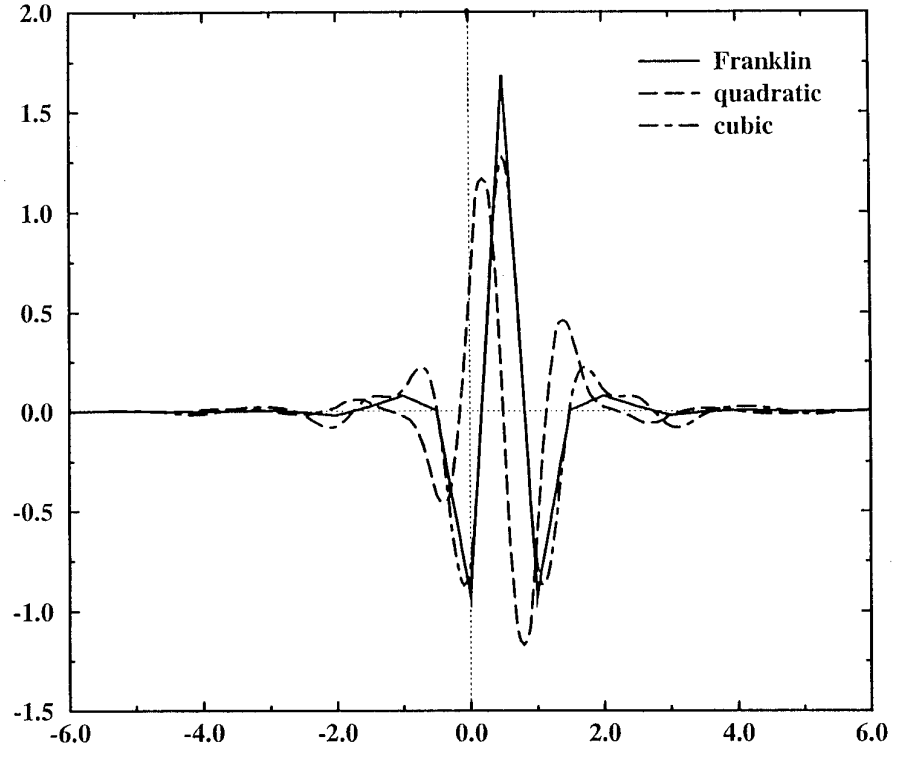

FIG. 7. Mother wavelet of the Franklin, quadratic, and cubic Lemarie–Meyer wavelets for $L^2(\Re)$.

TABLE IV

H Filter for Franklin Wavelet

n	0	1	2	3	4
h_n	0.817639	0.397295	−6.90964E-2	−5.19436E-2	1.69705E-2
n	5	6	7	8	9
h_n	9.99035E-3	−3.88322E-3	−2.20192E-3	9.24030E-4	5.12733E-4
n	10	11	12	13	14
h_n	−2.23886E-4	−1.22829E-4	5.53061E-5	3.00401E-5	−1.38087E-5
n	15	16	17	18	19
h_n	−7.45399E-6	3.53383E-6	2.48447E-6	2.17113E-7	−1.22248E-8

enough so that $2^{-j}\max(L_\phi, L_\psi) < 1$, where L_ϕ and L_ψ are the supports of ϕ and ψ, and the wavelets are (a)symmetric, then $\overline{\phi}$ and $\overline{\psi}$ are obtained as

$$\overline{\phi}_{jk} = \begin{cases} \phi_{jk} & \text{if } L_\phi/2 < k < 2^j - L_\phi/2 \\ \phi_{jk} + \phi_{j,k+2j} & \text{if } k < L_\phi/2 \\ \phi_{jk} + \phi_{j,k-2j} & \text{if } k > 2^j - L_\phi/2; \end{cases} \tag{66}$$

$$\overline{\psi}_{jk} = \begin{cases} \psi_{jk} & \text{if } L_\psi/2 < k < 2^j - L_\psi/2 \\ \psi_{jk} + \psi_{j,k+2j} & \text{if } k < L_\psi/2 \\ \psi_{jk} + \psi_{j,k-2j} & \text{if } k > 2^j - L_\psi/2. \end{cases} \tag{67}$$

A function $f(x) \in L^2([0,1])$ can then be approximated as

$$f(x) \approx f_n(x) = \sum_{k=0}^{2^n-1} c_{nk} \sum_{\ell \in Z} \phi_{n,k+2^j\ell} \tag{68}$$

or

$$f_n(x) = \sum_{k=0}^{2^{n_0}-1} c_{n_0 k} \sum_{\ell \in Z} \phi_{n,k+2^j\ell} + \sum_{j=n_0}^{n} \sum_{k=0}^{2^j-1} d_{j,k} \sum_{\ell \in Z} \psi_{j,k+2^j\ell}, \tag{69}$$

where $n_0 \geq 0$.

TABLE V

a_k, the Triangle Decomposition of the Father Franklin Wavelet $\phi(x)$

k	0	1	2	3	4
a_k	1.29167	−0.174658	3.52093E-2	−7.87426E-3	1.84791E-3
k	5	6	7	8	9
a_k	−4.45912E-4	1.09575E-4	−2.72725E-5	6.85273E-6	−1.73453E-6

TABLE VI

b_k, the Triangle Decomposition of the Mother Franklin Wavelet $\psi(x)$

k	0	1	2	3	4
b_k	1.68193	−0.927157	0.495137-2	7.74402E-2	2.37810E-2
k	5	6	7	8	9
b_k	−1.96407E-2	−4.64087E-3	4.12684E-3	1.19977E-3	−9.81160E-4
k	10	11	12	13	14
b_k	−2.91486E-4	2.35038E-4	7.28989E-5	−5.76965E-5	−1.82992E-5
k	15	16	17	18	19
b_k	1.43298E-5	4.63154E-6	−3.59569E-6	−1.17852E-6	9.09006E-7

ACKNOWLEDGMENTS

This research was supported in part with funds from DARPA/ESTO under Grants N00014-91-J-4030 from the Office of Naval Research, N66001-89-C-0104 from NCCOSC/NRaD, and from Boeing Aerospace Company under Contract 133-P771. The authors thank Dr. B. Gilbert (Mayo Foundation), Dr. J. Murphy (DARPA/ESTO), Dr. R. Pohanka and Dr. L. Kabacoff (ONR), and Dr. P. Young (Boeing High Technology Center) for support. They also thank Mr. Mikhail Toupikov of the Department of Electrical Engineering, Arizona State University, for helpful discussions and preparation of text and figures.

REFERENCES

1. G. Pan, J. Prentice, S. Kahn, A. Staniszewski, W. Walters, and B. Gilbert, The simulation of high-speed, high-density digital interconnects in single chip packages and multichip modules, *IEEE Trans. Comput. Hyb. Manuf. Technol.* **15**(4), 465 (1992).
2. J. J. Benedette and M. W. Franzier, *Wavelets: Mathematics and Applications* (CRC Press, Ann Arbor, MI, 1994).
3. B. K. Alpert, Wavelets and other bases for fast numerical linear algebra, in *Wavelets: A Tutorial in Theory and Applications,* edited by C. K. Chui (Academic Press, New York, 1992).
4. S. Jaffard and Ph. Laurencot, Orthonormal wavelets, analysis of operators, and applications to numerical analysis, in *Wavelets: A Tutorial in Theory and Applications,* edited by C. K. Chui (Academic Press, New York, 1992).
5. R. Glowinski, W. Lawton, M. Ravachol, and E. Tenenbaum, Wavelet solutions of linear and nonlinear elliptic, parabolic, and hyperbolic problems in one space dimension, in *Computational Methods in Applied Science and Engineering,* edited by R. Glowinski (SIAM, Philadelphia, 1990).
6. G. Beylkin, R. Coifman, and V. Roklin, Fast wavelet transforms and numerical algorithm I, *Commun. Pure Appl. Math.* **44,** 141 (1991).
7. B. Z. Steinberg and Y. Leviatan, On the use of wavelet expansion in the method of moments, *IEEE Trans. Antenna Propagat.* **41**(5), 610 (1993).
8. K. Sabetfakhri and L. Katehi, Analysis of integrated millimeter-wave and submillimeter-wave waveguides using orthonormal wavelet expansions, *IEEE Trans. Microwave Theory Technique* **42,** 2412 (1994).
9. G. Pan and X. Zhu, The application of fast adaptive wavelet expansion

method in the computation of parameter matrices of multiple lossy transmission lines, in *IEEE Antennas Propagat. Society Symposium, June 1994,* pp. 29–32.

10. G. Wang and G. Pan, Full wave analysis of microstrip floating structures by wavelet expansion method, *IEEE Trans. Microwave Theory Technique* **43**(1), 131 (1995).
11. G. Wang, G. Pan, and B. Gilbert, A hybrid wavelet expansion and boundary element analysis for multiconductor transmission line in multilayered dielectric media, *IEEE Trans. Microwave Tech.* **43**(3), 664 (1995).
12. G. Pan, Orthogonal wavelets with applications in electromagnetics, *IEEE Trans. Magn.* **32**(3), 975 (1996).
13. G. Pan, J. Du, and B. Gilbert, Application of intervallic wavelets to the surfare integral equations, *IEEE Trans. Antennas Prop.,* submitted.
14. M. Toupikov and G. Pan, On the use of weighted wavelet expansions for integral equations on bounded intervals, *IEEE Trans. Antennas Prop.,* submitted.
15. I. Daubechies, *Ten Lectures on Wavelets* (SIAM, Philadelphia, 1992).
16. J. Stratton, *Electromagnetic Theory* (McGraw–Hill, New York, 1941), p. 359.
17. F. Olyslager, D. D. Zutter, and K. Blomme, Rigorous analysis of the propagation characteristics of general lossless and lossy multiconductor transmission lines in multilayered media, *IEEE Trans. Microwave Theory Technique* **41**(1), 79 (1993).
18. R.-B. Wu and J.-C. Yang, Boundary integral equation formulation of skin effect problems in multiconductor transmission lines, *IEEE Trans. Magn.* **MAG-25,** 3013 (1989).
19. M. J. Tsuk and J. A. Kong, A hybrid method for the calculation of the resistance and inductance of transmission lines with arbitrary cross sections, *IEEE Trans. Microwave Theory Technique* **39**(8), 1338 (1991).
20. G. Beylkin, R. Coifman, and V. Roklin, Wavelets in numerical analysis, in *Wavelets and Their Applications,* edited by M. B. Ruskai (Jones & Bartlett, Boston, 1992).
21. C. C. Paige and M. A. Sounders, LSQR: An algorithm for sparse linear equations and sparse least squares, *ACM Trans. Math. Software* **8**(1), 43 (1982).
22. G. Golub and C. Van Loan, *Matrix Computations* (John Hopkins Univ. Press, Baltimore, MD, 1983).
23. J. A. Dobrowolski, *Introduction to Computer Methods for Microwave Circuit Analysis and Design* (Artech House, Norwood, MA, 1991).
24. L. A. Hagman and D. M. Young, *Applied Iterative Methods* (Academic Press, New York, 1981).
25. R. Faraji-Dana and Y. Chow, Edge condition of the field and a.c. resistance of a rectangular strip conductor, *IEE Proc.* **137,** Pt. H(2), 133 (1990).
26. G. Pan, K. Olson, and B. Gilbert, Improved algorithmic methods for the prediction of wavefront propagation behavior in multiconductor transmission lines for high frequency digital signal processors, *IEEE Trans. CAD Int. Circ. Systems* **8**(6), 608 (1989).
27. G. G. Walter, *Wavelets and Other Orthogonal Systems with Applications,* University of Wisconsin-Milwaukee, 1993.
28. C. K. Chui, *An Introduction to Wavelets* (Academic Press, New York, 1991).
29. S. Mallat, A theory of multiresolution decomposition: the wavelet representation, *IEEE Trans. Pattern Anal. Mach. Intell.* **11**(7), 674 (1989).